JOURNAL OF GUIDANCE, CONTROL, AND DYNAMICS
Vol. 22, No. 6, November–December 1999

Spacecraft Spin Stabilization Using a Transverse Wheel for Any Inertia Ratio

Richard A. Fowell,* Richard I. Milford,† and John F. Yocum‡
Hughes Space and Communications Company, El Segundo, California 90245

Hughes Space and Communications Company recently launched the first of a series of satellites featuring a patented control strategy capable of stabilizing spin about a given spacecraft axis, regardless of spin-to-transverse inertia ratio. The control system, which functions during the ascent phase of the mission, makes use of on-station control hardware, a gyro and a transverse reaction wheel, to stabilize spin. This is believed to be the first instance of stabilization of spin with arbitrary inertia ratio using a single transverse wheel. For stability reasons, these satellites are the first Hughes satellites to spin negatively in transfer orbit. It is paradoxical that, for some inertia ratios, negative spin can be stabilized when positive spin cannot. Note that, in such cases, even the negative spin, though stable, may be technically uncontrollable at one point in the mission. The history of active spin control is discussed, and some global principles for spin stabilization using a single wheel are established. Theory, design, and flight experience of the Hughes active spin controller are presented and contrasted to prior solutions. Finally, ground simulations and flight telemetry are presented and compared.

Introduction

THE spin stabilization system for the Hughes Space and Communications Company high-power communications spacecraft, model HS601HP, is designed to stabilize spin about the ascent motor thrust axis. Spin stabilization during transfer orbit is attractive compared to 3-axis stabilization because it provides a benign thermal environment, requires less control equipment, and has relatively simple failure response scenarios. To maximize equipment layout flexibility, the spin stabilization is required to work whether the spin axis inertia is major, minor, or intermediate. All three conditions can occur in a single ascent because the large mass of fuel expended during ascent greatly changes the inertias. To minimize fuel consumption and onboard equipment, the primary spin stabilization system avoids thrusters and uses only sensors and actuators that exist for on-station control (the gyro and momentum wheel). This is believed to be the first instance of intermediate axis spin stabilization using a single transverse wheel.

From a dynamics point of view, it is most convenient to spin a satellite about the principal axis of greatest inertia, major axis spin, because this is inherently stable. However, launch vehicle stowage volumes are usually long and narrow, and this provides an incentive to spin a satellite about its long axis, the principal axis of least inertia. This minor axis spin equilibrium is a high-energy state and is unstable to the extent that energy dissipation mechanisms (principally fluid motion) act on the satellite. To stabilize minor axis spin, a spin axis stabilization (or nutation) control system is used. Because the instability of minor axis spin can be made relatively mild (oscillatory with slow growth), many satellites have been minor axis spinners during ascent. Whereas spin about the axis of intermediate principal inertia is an equilibrium, it is an unstable equilibrium, with or without dissipative mechanisms. It is exponentially divergent with a time constant on the same order as the spin period. Because of this strong instability, intermediate axis spin has usually been avoided in the past.

Satellite nutation control systems using a single fixed transverse wheel to stabilize minor axis spin have a long history. Such a system was described by Beusch and Smith[1] in 1970, by Perkel in 1971,[2] and flown on LAGEOS in 1976.[3,4] More recently, MSAT flew such a system in April 1995, and Galaxy IIIR used a similar design in combination with momentum augmentation at $\frac{1}{3}$ rpm in December 1995.[5] However, no literature was found suggesting the use of a single transverse wheel for active feedback control of intermediate axis spin.

Two techniques that have been used in space to stabilize intermediate axis spin or similar instabilities are momentum augmentation and two-axis thruster control. During part of the Intelsat VI ascent (1989), the satellite as a whole had its intermediate moment of inertia along the spin axis. The oblate section of the satellite that is despun in operation (the platform) was spun to a higher speed than the rotor to achieve a two-body dynamic state analogous to major axis spin.[6] Similar approaches using internal wheels can be used to convert the intermediate axis spin equilibrium to an equilibrium analogous to major or minor axis spin by adding or subtracting momentum about the spin axis.[7,8] This system was flown on Galaxy IIIR.[5] If enough momentum is added, the desired spin direction is globally stable in the presence of energy dissipation.[7,9,10] Two-axis thruster stabilization of intermediate axis spin has also been analyzed[11] and flown for brief periods.

An initial reaction to the suggestion that a single transverse wheel could be used to stabilize intermediate axis spin was that two wheels seemed to be necessary. Analysis showed that, indeed, a single fixed transverse wheel cannot stabilize a given sign of intermediate axis spin for arbitrary mass properties. However, the range of mass properties seen during an ascent is limited enough that, if the sign of spin can be chosen appropriately, the satellite spin is stabilizable throughout ascent, although it is not controllable throughout.

Spacecraft Dynamics Analysis

This section presents a discussion of the spacecraft dynamics, with emphasis on intermediate axis spin. It derives an analytical model and seeks to extract from that model some physical insight into the behavior of an intermediate axis spinner.

Equations of Motion

Consider a spacecraft, shown in Fig. 1, comprising a rigid body with spin rate ω, to which is attached a single momentum wheel with its unit spin axis $\hat{\boldsymbol{w}}$ defined by the angle β in the spacecraft's 1–2 plane. The axes $\{\hat{\boldsymbol{p}}_1, \hat{\boldsymbol{p}}_2, \hat{\boldsymbol{p}}_3\}$ are the spacecraft principal inertia axes and Fig. 1 shows a body spinning about its intermediate moment-of-inertia (MOI) axis $\hat{\boldsymbol{p}}_3$ because this configuration is the primary

Received 13 July 1998; presented as Paper 98-4434 at the AIAA Guidance, Navigation, and Control Conference, Boston, MA, 10–12 August 1998; revision received 4 April 1999; accepted for publication 4 April 1999.

*Senior Scientist, Command and Control Subsystems. Senior Member AIAA.
†Senior Staff Engineer, Command and Control Subsystems. Member AIAA.
‡Chief Scientist, Command and Control Subsystems.

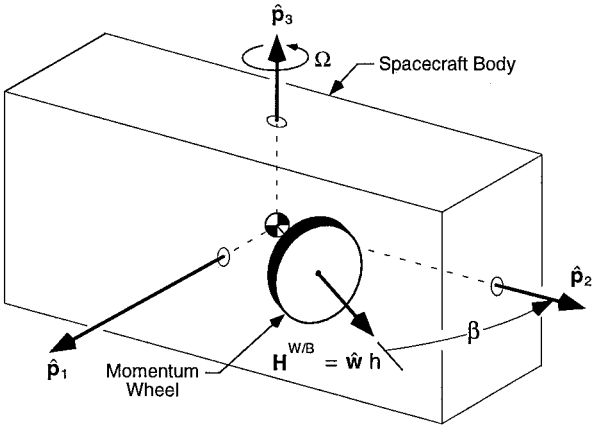

Fig. 1 Spacecraft model: rigid body plus momentum wheel.

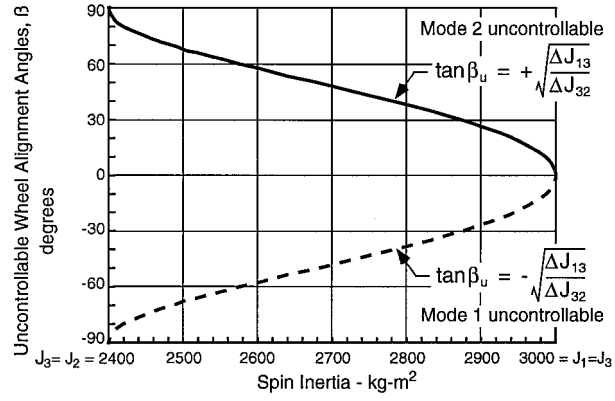

Fig. 2 Typical variation of uncontrollable wheel alignment over mission.

focus in this paper. The rigid-body equations of motion for such a spacecraft are

$$\begin{aligned} L_1 &= J_1\dot{\omega}_1 + \dot{h}s\beta + (J_3 - J_2)\omega_2\omega_3 - h\omega_3 c\beta \\ L_2 &= J_2\dot{\omega}_2 + \dot{h}c\beta + (J_1 - J_3)\omega_1\omega_3 - h\omega_3 s\beta \\ L_3 &= J_3\dot{\omega}_3 + (J_2 - J_1)\omega_1\omega_2 + h\omega_1 c\beta - h\omega_2 s\beta \end{aligned} \tag{1}$$

where $(\dot{})$ indicates differentiation with respect to time, $\{J_1, J_2, J_3\}$ are the principal moments of inertia; $\{L_1, L_2, L_3\}$ and $\{\omega_1, \omega_2, \omega_3\}$ are external torques and body angular rates, both expressed in body axes; and h is the scalar angular momentum in the wheel relative to the spacecraft body. The notation $s\beta$ and $c\beta$ denotes $\sin(\beta)$ and $\cos(\beta)$.

From Eq. (1), one may deduce the well-known result that, in the absence of external torques and with $h = 0$, a nontrivial constant solution exists for motion about any one of the three principal axes. Consider the solution where $\omega_1 = \omega_2 = h = 0$ and $\omega_3 = \Omega = a$ constant. By linearizing the equations about this solution and defining of the body momentum components $h_1^B = J_1\omega_1$, $h_2^B = J_2\omega_2$, and $h_3^B = J_3\omega_3$, one obtains the following linearized equations for torque free motion:

$$\begin{aligned} \dot{h}_1^B &= (J_2 - J_3)\Omega h_2^B \big/ J_2 + \Omega h c\beta - \dot{h}s\beta \\ \dot{h}_2^B &= (J_3 - J_1)\Omega h_1^B \big/ J_1 - \Omega h s\beta - \dot{h}c\beta, \qquad \dot{h}_3^B = 0 \end{aligned} \tag{2}$$

For these dynamics, we envision a control system wherein the control u is proportional to the wheel torque:

$$u = \dot{h} \tag{3}$$

Combining Eqs. (2) and (3), one obtains the following linear state-space equations describing the spacecraft nutational dynamics:

$$\begin{Bmatrix} \dot{h}_1^B \\ \dot{h}_2^B \\ \dot{h} \end{Bmatrix} = \begin{bmatrix} 0 & -\mu_{12}\Delta J_{32}\Omega & \Omega c\beta \\ -\Delta J_{13}\Omega/\mu_{12} & 0 & -\Omega s\beta \\ 0 & 0 & 0 \end{bmatrix} \begin{Bmatrix} h_1^B \\ h_2^B \\ h \end{Bmatrix} + \begin{Bmatrix} -s\beta \\ -c\beta \\ 1 \end{Bmatrix} u \tag{4}$$

where the following nondimensional parameter definitions apply: $\Delta J_{32} = (J_3 - J_2)/J_1$, $\Delta J_{13} = (J_1 - J_3)/J_2$, and $\mu_{12} = J_1/J_2$. Note that the parameters ΔJ_{32} and ΔJ_{13} have been defined with an intermediate MOI axis spin in mind. When J_3 is intermediate both parameters have the same sign and the product $\Delta J_{32} \cdot \Delta J_{13}$ is positive. Equation (4) casts the dynamics in a relatively simple standard state-space format to which the powerful tools of linear analysis may be readily applied.

Controllability

The system described by Eq. (4) has some interesting characteristics, which we explore in this section. Define a state, $\boldsymbol{x} = \{h_1^B \;\; h_2^B \;\; h\}^T$, and let $\boldsymbol{A}$ and $\boldsymbol{b}$ denote the coefficient matrices in Eq. (4). To determine if the system is controllable, one may check the rank of the controllability matrix:

$$\boldsymbol{Q}_c = [\boldsymbol{b} \quad \boldsymbol{Ab} \quad \boldsymbol{A}^2\boldsymbol{b}] \tag{5}$$

After a little algebra, one may show that

$$\det(\boldsymbol{Q}_c) \propto \Delta J_{32}\sin^2(\beta) - \Delta J_{13}\cos^2(\beta) \tag{6}$$

From Eq. (6), it is evident that the system becomes uncontrollable if the wheel is aligned at an angle β_u such that

$$\tan\beta_u = \pm\sqrt{\Delta J_{13}/\Delta J_{32}} \tag{7}$$

but otherwise it is completely controllable. In practice, the physical wheel alignment β is fixed, whereas the alignment leading to uncontrollability, β_u, varies with inertias as the spacecraft propellant is depleted during transfer orbit. Figure 2 shows β_u vs spin inertia as the spin inertia varies from maximum to minimum MOI. It illustrates that, in a worst-case mission, the range of β_u covers a full circle so that inertia variations will virtually guarantee that at some point an alignment corresponding to an uncontrollable situation will arise. However, an eigenanalysis of the system will lead to a better understanding of the implications of Eq. (7) and will show that, even in a worst-case mission when the system is uncontrollable, a stable control system is still possible.

Because the system is fairly simple, one can analytically determine the eigenvalues and eigenvectors. The eigenvalues of $\boldsymbol{A}$ are

$$\lambda = \left(+\Omega\sqrt{\Delta J_{13}\Delta J_{32}}, \qquad -\Omega\sqrt{\Delta J_{13}\Delta J_{32}}, \qquad 0\right) \tag{8}$$

and the corresponding eigenvectors (in columns) are

$$\boldsymbol{V} = \begin{bmatrix} \mu_{12}\sqrt{\Delta J_{32}} & \mu_{12}\sqrt{\Delta J_{32}} & -\mu_{12}\Delta J_{32}s\beta \\ -\sqrt{\Delta J_{13}} & \sqrt{\Delta J_{13}} & \dfrac{\Delta J_{13}c\beta}{\mu_{12}} \\ 0 & 0 & \Delta J_{32}\Delta J_{13} \end{bmatrix} \tag{9}$$

Note that, if J_3 is maximum or minimum MOI, then the two nonzero eigenvalues are imaginary, representing oscillatory motion (generally called nutation), and the eigenvectors are complex. For the case of primary interest here, J_3 is the intermediate MOI axis, and the eigenvalues and eigenvectors are real. One of the eigenvalues is in the left-half plane, representing a stable exponential mode, whereas

one is in the right-half plane representing a divergent exponential mode.

Equation (9) may be used to perform a modal coordinate transformation

$$\boldsymbol{x} = \boldsymbol{V}\boldsymbol{\eta} \tag{10}$$

to diagonalize the system. The result is

$$\dot{\boldsymbol{\eta}} = \boldsymbol{A}^{\eta}\boldsymbol{\eta} + \boldsymbol{b}^{\eta}u \tag{11}$$

where $\boldsymbol{A}^{\eta}$ is diagonal and contains the eigenvalues of $\boldsymbol{A}$

$$\boldsymbol{A}^{\eta} = \boldsymbol{V}^{-1}\boldsymbol{A}\boldsymbol{V} = \begin{bmatrix} \Omega\sqrt{\Delta J_{32}\Delta J_{13}} & 0 & 0 \\ 0 & -\Omega\sqrt{\Delta J_{32}\Delta J_{13}} & 0 \\ 0 & 0 & 0 \end{bmatrix} \tag{12}$$

and the transformed control input vector $\boldsymbol{b}^{\eta}$ is given by

$$\boldsymbol{b}^{\eta} = \boldsymbol{V}^{-1}\boldsymbol{b} = \frac{1}{\Delta J_{32}\Delta J_{13}} \begin{Bmatrix} (J_3/J_1)\left(s\beta\sqrt{\Delta J_{32}} + c\beta\sqrt{\Delta J_{13}}\right) \\ (J_3/J_1)\left(s\beta\sqrt{\Delta J_{32}} - c\beta\sqrt{\Delta J_{13}}\right) \\ 1 \end{Bmatrix} \tag{13}$$

Examination of Eq. (13) sheds light on the controllability condition in Eq. (7). Evidently, if the wheel is aligned with

$$\beta = \beta_{u1} = -\arctan\left(\sqrt{\Delta J_{13}/\Delta J_{32}}\right) \tag{14}$$

then the first mode, with the eigenvalue at $\lambda = +\Omega\sqrt{(\Delta J_{32}\Delta J_{13})}$, is uncontrollable whereas the second and third modes are controllable. Likewise, if the wheel is aligned with

$$\beta = \beta_{u2} = +\arctan\left(\sqrt{\Delta J_{13}/\Delta J_{32}}\right) \tag{15}$$

then the second mode, with the eigenvalue at $\lambda = -\Omega\sqrt{(\Delta J_{32}\Delta J_{13})}$, is uncontrollable whereas the first and third modes are controllable.

Further insight may be gained by noting, from inspection of the eigenvectors in Eq. (9), the angles that the rate vectors associated with the two modes make with respect to the $\hat{\boldsymbol{p}}_2$ axis are

$$\tan\alpha_{\omega 1} = \left.\frac{\omega_1}{\omega_2}\right|_{\text{mode 1}} = \left.\frac{h_1^B/J_1}{h_2^B/J_2}\right|_{\text{mode 1}} = \frac{\mu_{12}\sqrt{\Delta J_{32}}/J_1}{-\sqrt{\Delta J_{13}}/J_2} = \frac{\sqrt{\Delta J_{32}}}{-\sqrt{\Delta J_{13}}} \tag{16}$$

$$\tan\alpha_{\omega 2} = \left.\frac{\omega_1}{\omega_2}\right|_{\text{mode 2}} = \left.\frac{h_1^B/J_1}{h_2^B/J_2}\right|_{\text{mode 2}} = \frac{\mu_{12}\sqrt{\Delta J_{32}}/J_1}{+\sqrt{\Delta J_{13}}/J_2} = \frac{\sqrt{\Delta J_{32}}}{+\sqrt{\Delta J_{13}}} \tag{17}$$

These define the directions in the body frame of the constant rate vectors of the two modes associated with the nonzero eigenvalues. Figure 3 shows the geometry of these rate vectors, often referred to as separatrices,[12] relative to the body principal axes and relative to the critical wheel alignment β_{u1} that causes mode 1 to become uncontrollable. The arrowheads on the separatrices indicate the direction of motion, assuming that the body spin rate Ω is positive. The directions are reversed when Ω is negative. Note that when the wheel is aligned such that mode 1 is uncontrollable, the wheel's spin axis is perpendicular to the separatrix defining mode 2, that is, $\beta_{u1} + \alpha_{\omega 2} = 90$ deg as shown in Figure 3. Conversely (and not shown in Fig. 3), when the wheel is aligned such that mode 2 is uncontrollable, the wheel's spin axis is perpendicular to the separatrix defining mode 1, that is, $\beta_{u2} + \alpha_{\omega 1} = 90$ deg.

Physical Interpretation of Uncontrollability

To gain a physical understanding of this behavior, one may contrast the intermediate axis spin dynamics and control problem with the major or minor axis spin dynamics and control problem. In the case of major or minor axis spin, the modes of motion are complex (as opposed to real) and coupled, one being 90 deg out of phase with the other. Moreover, the rate associated with a mode moves around

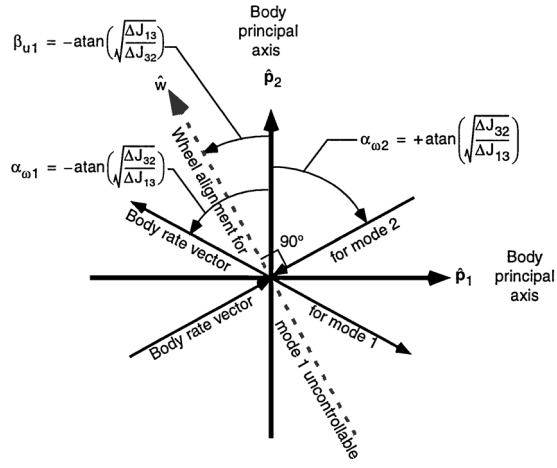

Fig. 3 Geometry showing wheel alignment leading to uncontrollable mode.

in the body (the transverse rate vector rotates at body nutation frequency). Thus, a momentum wheel placed at almost any orientation (except with the wheel spin axis parallel to the body spin axis) will be capable of producing torque to oppose the motion if one is simply smart enough to phase the torque properly with respect to the moving body rate vector. Because the modes are coupled, control of one mode implies control of the other. This is the basis for a nutation control system used on many spacecraft.

In the case of intermediate axis spin, the situation is much different. Both the wheel torque directions and the rate vectors defining the modes of motion are fixed in the body frame. The orientations of the modal rate vectors are determined by spacecraft mass properties, whereas the wheel torque directions are fixed independently by the wheel's alignment. Moreover, the two body modes are independent. For certain positions of the wheel, both modes are controllable; however, if the wheel is positioned incorrectly it may be possible to control one mode, but not the other.

To determine, through physical arguments, what the incorrect wheel orientation is, consider that the wheel exerts torques on the spacecraft body in two ways: 1) a direct torque component $\dot{h}\hat{\boldsymbol{w}}$ is exerted by the wheel spin motor, and 2) a gyroscopic torque $\boldsymbol{\omega} \times \boldsymbol{H}^{W/B}$ is generated by the wheel as the spinning body precesses the momentum vector of the spinning wheel. The torque $\dot{h}\hat{\boldsymbol{w}}$ is parallel to the wheel spin axis whereas $\boldsymbol{\omega} \times \boldsymbol{H}^{W/B}$ is perpendicular to it. In general, it is the $\boldsymbol{\omega} \times \boldsymbol{H}^{W/B}$ torque that performs control of the vehicle, whereas the $\dot{h}\hat{\boldsymbol{w}}$ torque serves to create and remove wheel momentum that enables the $\boldsymbol{\omega} \times \boldsymbol{H}^{W/B}$ torque to become effective. This notion is supported by simulation results that show that the $\boldsymbol{\omega} \times \boldsymbol{H}^{W/B}$ torque component is generally dominant. This differs from nutation control, where the wheel spin torque is used to pump the body energy state to a minimum (for major axis spin) or a maximum (for minor axis spin). The energy change is proportional to

$$\int \boldsymbol{\omega} \bullet \hat{\boldsymbol{w}}\dot{h}\,\mathrm{d}t$$

For intermediate axis spin, controlling the body's kinetic energy is insufficient, as the kinetic energy at the null is the same as that for the tumbling motion along the separatrices.

Given this insight, it is now clear that if the wheel spin axis is perpendicular to the stable mode as shown in Fig. 4, then the $\boldsymbol{\omega} \times \boldsymbol{H}^{W/B}$ torque is parallel to the stable mode separatrix, and that mode is directly controllable by the $\boldsymbol{\omega} \times \boldsymbol{H}^{W/B}$ torque component [see Initial Condition 1 (I.C. 1) in Fig. 4]. Now, with the same wheel orientation, consider an initial condition wherein only the unstable mode is excited (I.C. 2 in Fig. 4). Note that one component of the mode is parallel to $\boldsymbol{\omega} \times \boldsymbol{H}^{W/B}$ and can be controlled, whereas the other component is perpendicular to $\boldsymbol{\omega} \times \boldsymbol{H}^{W/B}$ and cannot be controlled. The resultant motion will diverge along the unstable separatrix if no control is applied, or along the direction of the wheel spin axis if control is applied to null the controllable component, which is perpendicular to the spin axis.

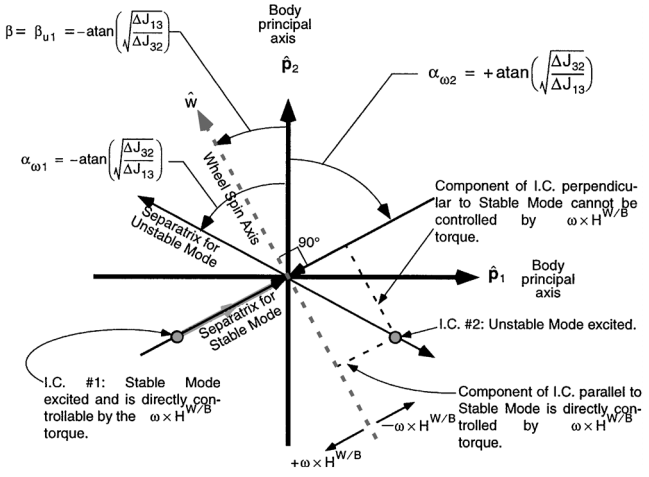

Fig. 4 Wheel aligned such that unstable mode is uncontrollable.

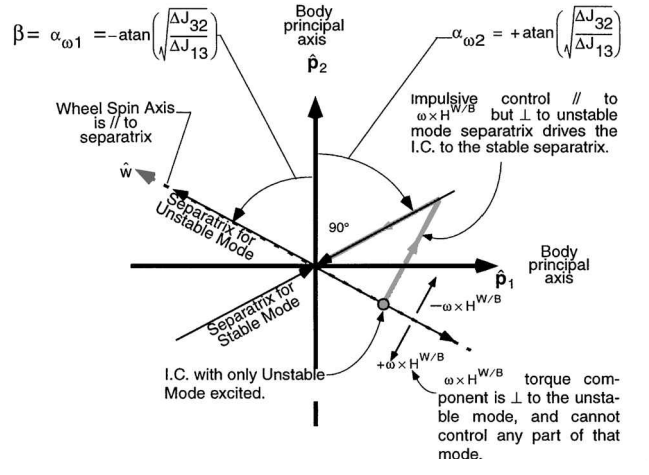

Fig. 5 Wheel aligned parallel to unstable mode: unstable mode remains controllable.

One might have expected that a mode becomes uncontrollable when the wheel is aligned parallel to its rate vector, for this would result in a geometry where the $\boldsymbol{\omega} \times \boldsymbol{H}^{W/B}$ torque component is perpendicular to the rate vector and, therefore, unable to control any component of the mode. This expectation is incorrect, as shown in Fig. 5, which shows a wheel alignment parallel to the separatrix of the unstable mode. Consider an initial condition wherein only the unstable mode is excited. Figure 5 shows that, while the $\boldsymbol{\omega} \times \boldsymbol{H}^{W/B}$ torque is perpendicular to the unstable mode, it can still be used to drive the initial condition along a path perpendicular to that mode until the rate lies on the separatrix of the stable mode, after which the motion will decay to null of its own accord. Thus, we see that the condition of uncontrollability for a given mode occurs when the $\boldsymbol{\omega} \times \boldsymbol{H}^{W/B}$ control torque is parallel to the separatrix of the other mode, not when it is perpendicular to the separatrix of the given mode.

These observations raise an interesting prospect. Suppose we have a design situation where the physical wheel alignment lies somewhere in the range from 0 to −90 deg. It is clear from Fig. 2 and Eq. (13) that the first mode, with eigenvalue at $\lambda = +\Omega\sqrt{(\Delta J_{32}\Delta J_{13})}$, will experience a condition of uncontrollability at some point in the mission. If we select a positive spin rate Ω, then the first mode is also unstable, a very bad situation indeed. However, by choosing to fly the mission with a negative spin rate, we will cause the first mode to be the stable one. Thus, that the first mode is uncontrollable at one point is immaterial. It is still stable. At the same time, the second mode with eigenvalue at $\lambda = -\Omega\sqrt{(\Delta J_{32}\Delta J_{13})}$ becomes unstable. This is tolerable, however, because that mode is now controllable over the entire mission via feedback through the control $u = \dot{h}$. This is an unusual phenomenon wherein one's ability to stabilize the control loop is critically dependent on the direction of spin. With positive spin in the example cited, a stable control loop throughout the mission is not possible, whereas with negative spin it is. This unusual phenomenon is not encountered when J_3 is either the minimum or maximum MOI axis. In these latter cases, one's ability to stabilize the system via feedback is independent of the direction of spin.

Controller Design and Flight Results

In this section, the detailed spin stabilization design for the HS601HP spacecraft is presented, based on the stability criteria developed in the preceding section. The controller synthesis is presented, followed by performance predictions, and finally flight results.

HS601HP Communications Satellite

The Hughes Space and Communications Company HS601HP satellite is a high-power geosynchronous communications satellite series, the first four of which were launched in 1997. Figure 6 shows an HS601HP satellite in its stowed transfer orbit configuration. Whereas all satellites in the series are similar, Astra 1G is of particular interest because it separated from the booster spinning about its intermediate MOI axis. Figure 7 shows, as a function of mission events, the maximum and minimum inertia ratios for the Astra 1G satellite. After the first apogee raising maneuver (AMF), fuel depletion caused the spin axis to transition to the minor axis of inertia. Once the spacecraft reached geosynchronous orbit, the

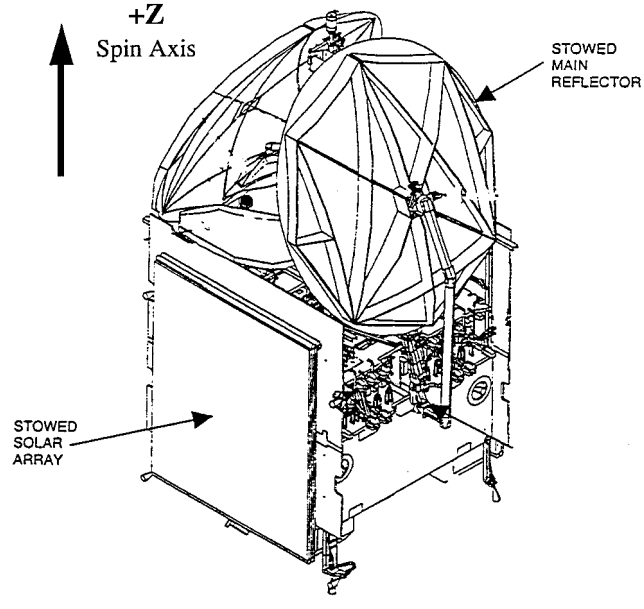

Fig. 6 HS601HP satellite in stowed configuration.

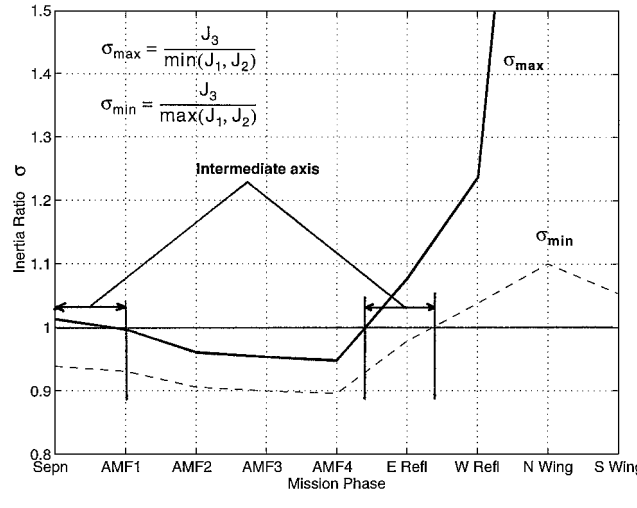

Fig. 7 Spin-to-transverse inertia ratio vs mission phase.

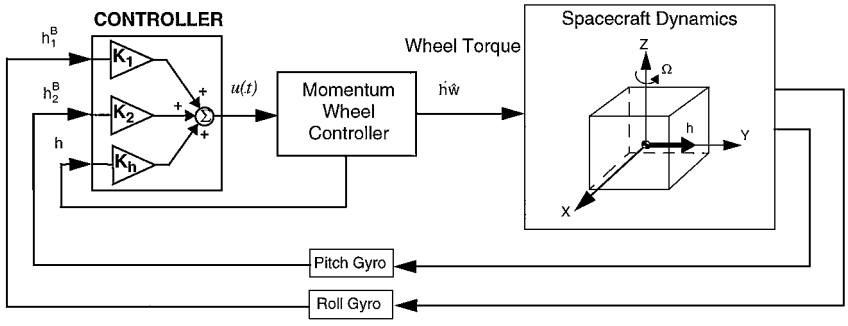

Fig. 8 Control system block diagram.

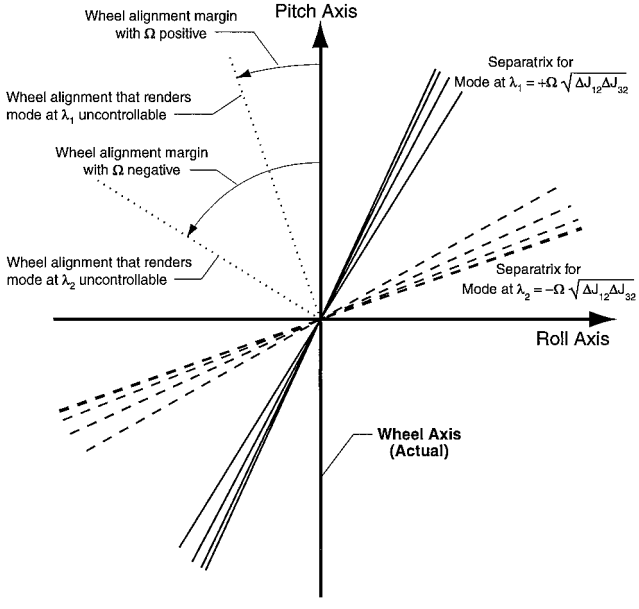

Fig. 9 Controllability vs mission phase.

communications reflectors and solar panels were deployed, during which time the spin axis transitioned up through intermediate to major axis. Figure 7 shows that the spacecraft layout, together with the mass properties changes associated with fuel depletion (over 1000 kg of propellent), resulted in a spacecraft that exhibited spin in all inertia ratio regimes (major/minor/intermediate) during the transfer orbit.

Feedback Controller Design

The intermediate and minor axis spin phases necessitate the use of active control for most of the mission. To minimize cost, the control system utilizes existing sensors and actuators, i.e., units required for on station control. To minimize fuel usage, a momentum wheel control actuator was selected over thrusters. Figure 8 shows a block diagram of the controller that was developed.[13] Spacecraft rates are sensed by a 3-axis inertial reference unit, and control torque is generated by a single momentum wheel, whose spin axis is perpendicular to the spacecraft spin axis. The flight processor implements the stabilizing control law and outputs a torque command to the momentum wheel. The momentum wheel speed is controlled via a digital tachometer loop. Both control loops operate at an 8-Hz sample rate. Sampling effects and high-frequency filter dynamics are not modeled here because they are second order with respect to stability and performance. However, such second-order effects are included in simulations.

On-station control of the satellite employs a single momentum wheel actuator aligned with its spin axis along the spacecraft pitch axis Y. This orientation is orthogonal to the transfer orbit spin axis Z, which is parallel to the liquid apogee motor thrust axis. Whereas this wheel alignment is reasonably well suited for spin stabilization, its predetermined orientation allows no room for optimizing

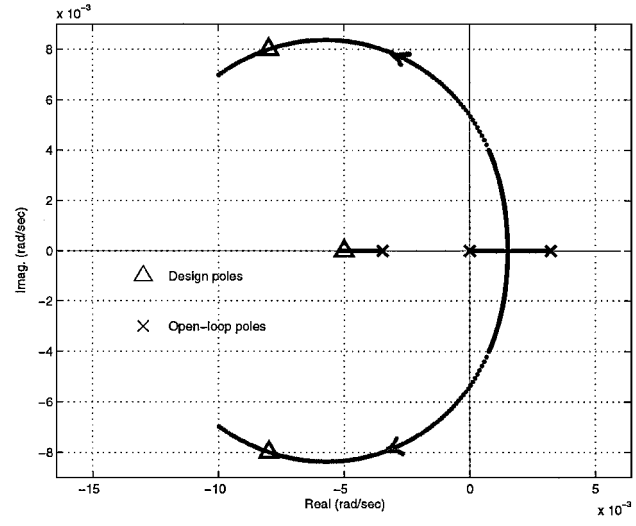

a) Root locus at design point

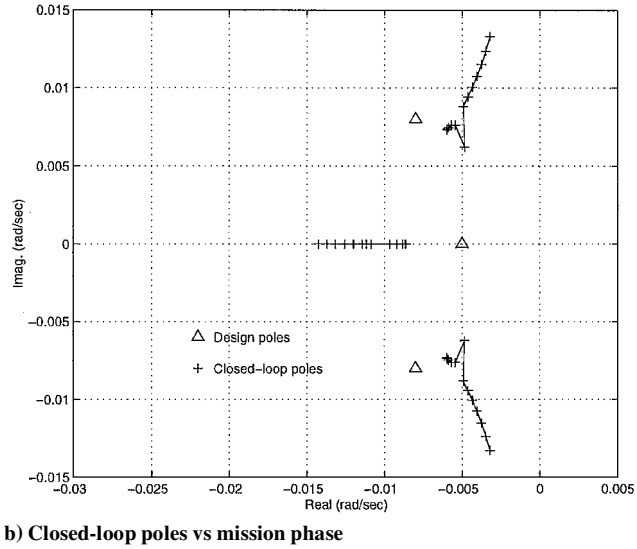

b) Closed-loop poles vs mission phase

Fig. 10 Closed-loop plant poles.

controllability by choosing its orientation with respect to spacecraft principal axes, as described in earlier sections.

The wheel orientation, combined with spacecraft mass properties, resulted in unfavorable stability characteristics when the spacecraft spins positively about $+Z$. Figure 9 shows the physical controllability of the spacecraft based on the concepts described earlier. Figure 9 shows the alignment of the wheel relative to the separatrices and indicates the two alignment angles that result in uncontrollability of the respective modes. It shows that with positive spin, the wheel alignment is within 20 deg of allowing the unstable mode to become uncontrollable, whereas selecting negative spin improves the margin to 60 deg. Although it is still possible to stabilize the

spacecraft with positive spin, it is not possible to achieve controller robustness with a fixed gain design. Therefore, a negative Z spin direction was selected.

In deriving the equations of motion, it was shown that the essential dynamics can be represented with a 3 element state vector

$$\boldsymbol{x} = \begin{Bmatrix} h_1^B \\ h_2^B \\ h \end{Bmatrix} = \begin{Bmatrix} \text{roll axis body momentum} \\ \text{pitch axis body momentum} \\ \text{wheel spin momentum} \end{Bmatrix} \tag{18}$$

The state-space equations describing the vehicle dynamics were defined in standard state-space format in Eq. (4). The feedback control law used to compute wheel torques is

$$u(t) = \dot{h}(t) = -\boldsymbol{K}\boldsymbol{x}(t) \tag{19}$$

showing that the commanded wheel torque is a linear combination of both transverse angular momentum components (roll and pitch) and the momentum wheel angular momentum. The state matrices vary significantly over the entire mission; however, the variation is slow enough that they can be treated as time invariant at any given point in time. After selecting a negative spin direction to maximize controllability of the unstable mode, a number of approaches could be used to design the feedback control law. Here, the control gain matrix $\boldsymbol{K}$ is calculated using a robust pole placement method, where the design objectives were to minimize control effort, avoid motor torque saturation, and achieve robustness over the range of satellite inertias for the HS601HP product line. Details of the design implementation include the following.

1) The stable eigenvalue/pole [at $\lambda = +\Omega\sqrt{(\Delta J_{32}\Delta J_{13})}$ with Ω negative] is not significantly shifted at the selected design point. This affords a twofold benefit: a) It minimizes control effort because it avoids using any control effort to change the already stable dynamics. b) It minimizes perturbation of the closed-loop poles under mass properties variation.

2) Controller bandwidth is constrained to avoid actuator saturation under the known bounded disturbances. The momentum wheel saturates at 0.19 Nm, and it is desirable to avoid saturation if possible, even though the primary control torque is due to the $\omega \times \boldsymbol{H}^{W/B}$ torque component.

3) Gains were chosen to achieve approximately 0.7 closed-loop damping ratio at booster separation.

A point design was constructed corresponding to spacecraft mass properties at the midpoint, with respect to fuel depletion, of the transfer orbit. The inertias used to compute the flight gains are based on early predictions of the spacecraft mass properties because the design had to be burnt into firmware early in the spacecraft development. Consequently, the actual closed-loop poles vary slightly in the as-launched configuration.

Figure 10a shows a root locus of the system wherein all three gains are varied proportionally. The unstable dynamics pole is forced into the left-hand plane whereas the stable dynamics pole is left nearly unchanged. The root contour plot in Fig. 10b shows the variation in closed-loop plant poles as a function of mission phase for the fixed gain design. Because of the large change in inertias, there is substantial perturbation of the closed-loop poles; however, the system

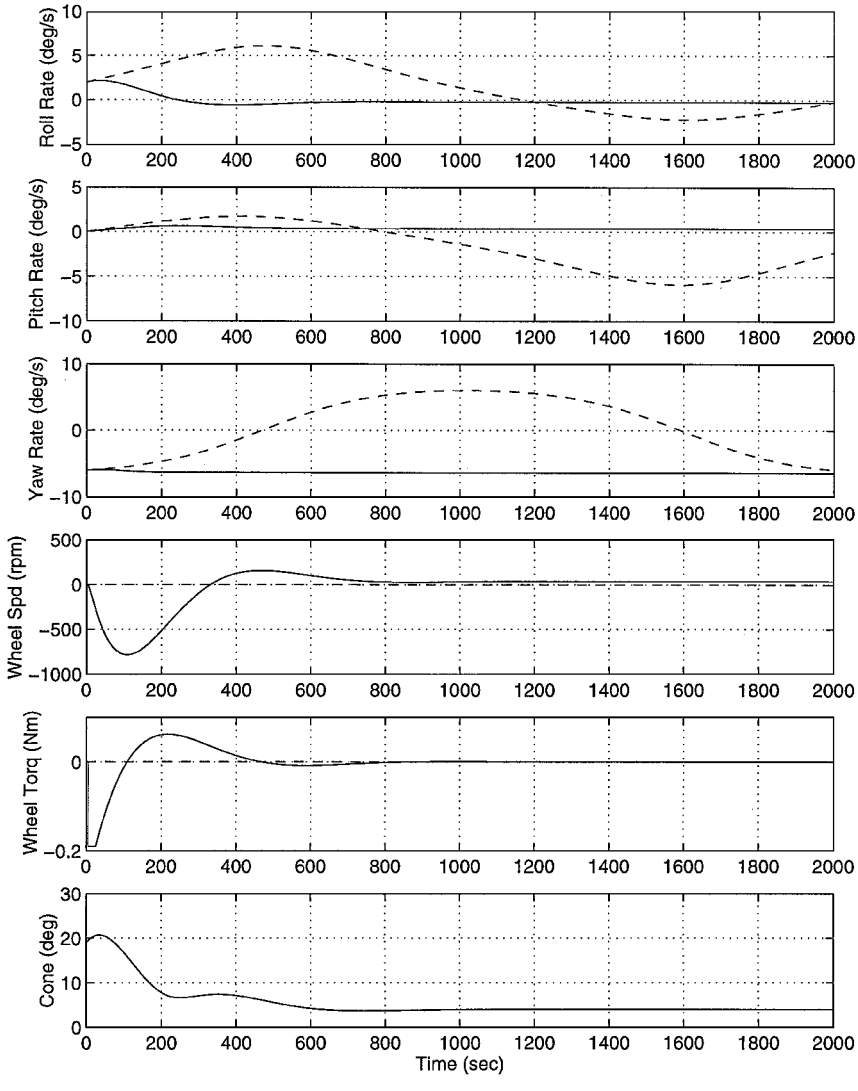

Fig. 11 Simulated booster separation: ——, closed loop, and – – –, open loop.

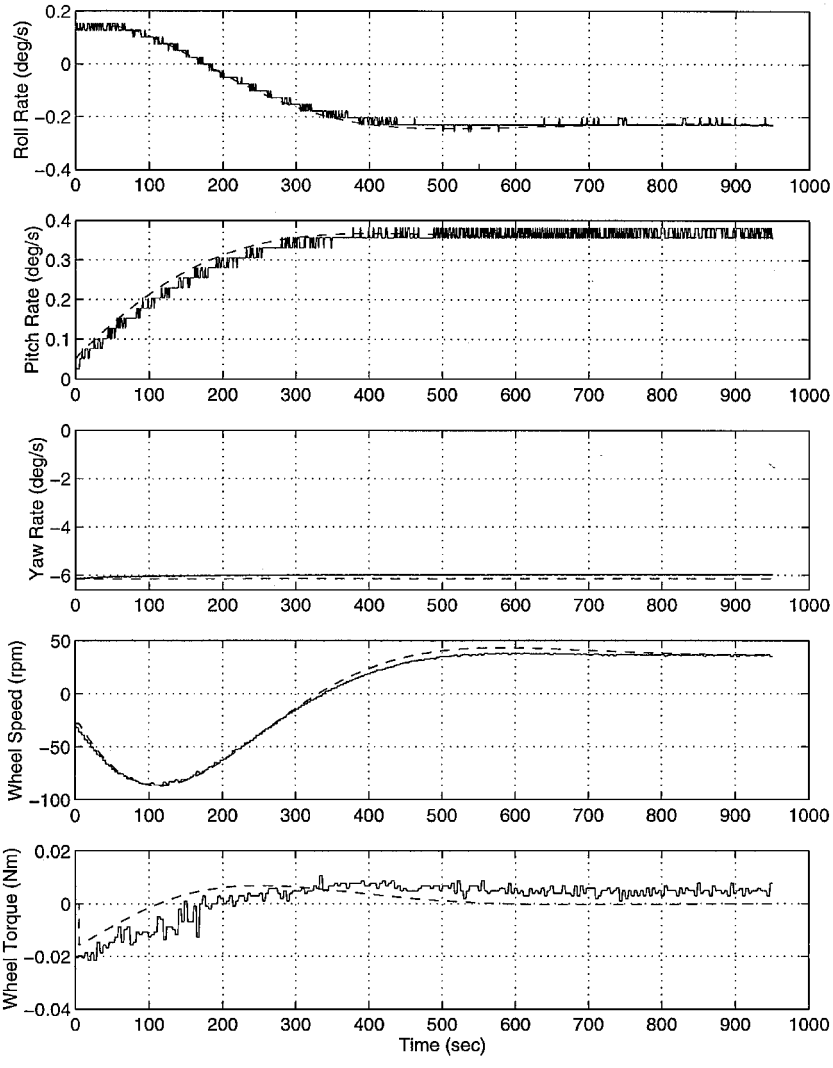

Fig. 12 Flight results; Astra 1G Booster Separation: ——, flight data, and - - - simulation.

remains stable with gain margin >8 dB and phase margin >45 deg throughout the transfer orbit using the fixed gain controller. For reference, the closed-loop poles corresponding to the design point are also indicated. Optimized gains can be uploaded, should it be desired to adjust performance, although this has not been necessary to date except during the deployments phase.

Controller Performance Predictions

Figure 11 shows a nonlinear simulation of the booster separation event when the control law is first initiated to stabilize spin about the spacecraft yaw axis. At separation, the Astra 1G yaw axis is intermediate with inertia matrix expressed in the body frame

$$I = \begin{bmatrix} 3433 & -130 & -10 \\ -130 & 3456 & 6 \\ -10 & 6 & 3357 \end{bmatrix} \text{kg-m}^2 \qquad (20)$$

and in the principal axis reference frame

$$J = \begin{bmatrix} 3314 & 0 & 0 \\ 0 & 3576 & 0 \\ 0 & 0 & 3356 \end{bmatrix} \text{kg-m}^2 \qquad (21)$$

A high-fidelity digital simulation environment is used, including a complete emulation of the flight code and detailed sensor/actuator models. The steady-state equilibrium spin exhibits 4 deg of coning because the spacecraft is not perfectly balanced about the yaw axis, as evident from the inertia matrix. The feedback controller yields the additional benefit of partially attenuating the steady-state coning; the coning is completely eliminated at a later stage during the mission, by appropriate configuration of the controlling momentum wheel and a second wheel.[5] Also shown in Fig. 11 is the open-loop response, which is a characteristic tumble (evident from yaw rate reversal) due to the intermediate axis spin; clearly this is undesirable.

Flight Results

Flight results are presented from the 1997 Astra 1G launch, where the spin stabilization control law, defined in Fig. 8, was implemented in flight hardware and software. The controller was autonomously activated at separation from the launch vehicle, which ejected the spinning spacecraft at −6 deg/s about the yaw axis and with a very small 0.15 deg/s transverse rate. Figure 12 shows telemetry from the separation event and subsequent spin stabilization under active wheel control. The response is slightly underdamped, taking about one closed-loop nutation period or 10 min for the transients to settle. Simulation results with matched initial conditions have been overlaid, from which it is clear that both the spacecraft dynamics and controller performance have been well characterized. Similar closed-loop performance is observed throughout the transfer orbit, with no discernible differences after the transition to minor axis, where the controller behaves more like a conventional nutation controller.

Figure 13 shows telemetry from the reflector deployment phase of the mission, which was performed using the same control system, but with optimized gains. As shown in Fig. 7, the satellite transitions from minor axis up through intermediate axis to major axis spin, covering all inertia ratio regimes during the deployment sequence.

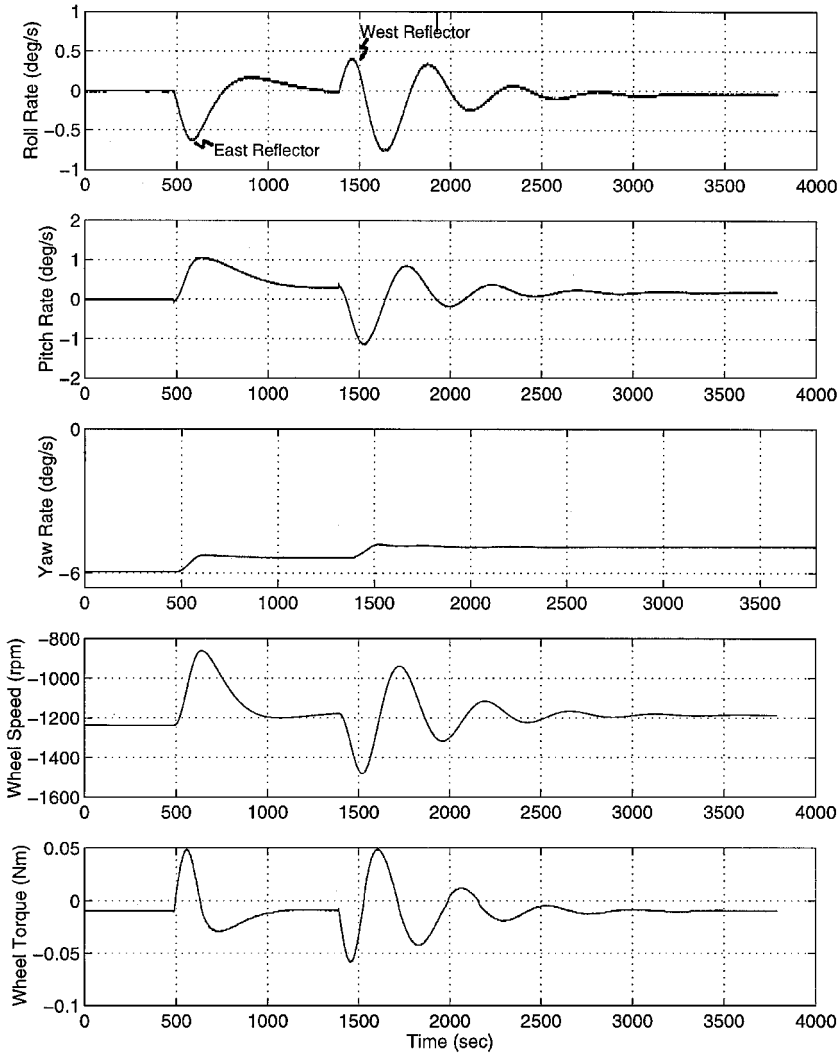

Fig. 13 Flight results; Astra 1G reflector deployments.

Conclusions

A single transverse momentum wheel, controlled with fixed gains based on sensed gyro rates, can stabilize satellite spin while the mass properties travel from minor axis spin, through intermediate axis spin, to major axis spin. It has been shown that, although stabilizability can be guaranteed, controllability cannot, resulting in a satellite whose direction of spin must be chosen to enhance stability. The preferred spin direction depends on spacecraft mass properties and wheel alignment. The flight results show that the flight control system built from this theory works in the practical world of propellant slosh, wobble, and structural flexure.

References

[1]Beusch, J. U., and Smith, N. P., "Stable Equilibria of a Freely Spinning Satellite Containing a Momentum Wheel in a Controlled Gimbal," AIAA Paper 70-982, Aug. 1970.

[2]Perkel, H., "Control System for Spinning Bodies," U.S. Patent 3,591,108, July 1971.

[3]Abercrombie, R. A., and Flatley, T. W., "An Active Nutation Damper for Spacecraft," *Proceedings of the 11th Aerospace Mechanisms Symposium*, NASA 1977, pp. 139–152.

[4]Hoffman, H. C., and Donohue, J. H., "Active Nutation Controller," U.S. Patent 4,193,570, March 1980.

[5]Salvatore, J., Barsky, M., and Quartararo, R., "Galaxy IIIR Transfer Orbit Attitude Control," *Proceedings of the Third International Conference on Spacecraft Guidance, Navigation and Control Systems*, ESA, Noordwijk, The Netherlands, 1996, pp. 361–365.

[6]Slafer, L. I., and Seidenstucker, V. L., "Attitude and Payload Control System for INTELSAT VI," *COMSAT Technical Review*, Vol. 21, No. 1, 1991, pp. 57–99.

[7]Hughes, P. C., *Spacecraft Attitude Dynamics*, Wiley, New York, 1986, Chaps. 6, 7.

[8]Salvatore, J. O., "Spin Stabilization via Momentum Wheels or Similar Devices," U.S. Patent 5,012,992, May 1991.

[9]Hubert, C. H., "Spacecraft Attitude Acquisition from an Arbitrary Spinning or Tumbling State," *Journal of Guidance and Control*, Vol. 4, No. 2, 1981, pp. 164–170.

[10]Hubert, C. H., "Orientation of Momentum Stabilized Vehicles," U.S. Patent 4,275,861, June 1981.

[11]Rosen, H. A., "Stabilization of a Spinning Spacecraft of Arbitrary Shape," U.S. Patent 4,961,551, Oct. 1990.

[12]Likins, P. W., *Elements of Engineering Mechanics*, McGraw–Hill, New York, 1973, p. 485.

[13]Fowell, R. A., and Yocum, J. F., "Satellite Spin Axis Stabilization Using a Single Degree of Freedom Transverse Momentum Storage Device," U.S. Patent 5,667,171, Sept. 1997.